# Heating of HMX-based PBXs during a low-velocity impact

David DROUET*, Didier PICART*, Eric BRUNETON*, Patrice BAILLY**

* CEA DAM, Le Ripault, F-37260 Monts, France
** Laboratoire Gabriel LaMé, INSA Centre Val de Loire, F-18000 Bourges, France

Corresponding author: david.drouet@cea.fr

## Abstract

The topic of non-shock initiation is still a challenge. In this domain, low-velocity impacts are one of the main accidental loadings which can lead to initiation. Nowadays, computers allow numerical simulations, instead of a lot of expensive and tedious tests. This eases the evaluation of the initiation risks in a large number of situations. Nevertheless the accuracy of numerical predictions depends on the physic embedded in the models and particularly, for initiation studies during mechanical loadings, on the heating mechanism. Indeed, if the consensus had grown around the concept of hot spot, the exact nature of the heat generating thermo-mechanical processes which preceded them remains unravelled.

We have focused our attention on Polymer Bonded Explosives (PBX) made of HMX (high melting point explosive) mixed with a few percent of a polymer binder. Recent experiments (reverse edge-on impact test) revealed the influence of the plasticity of HMX grains even for low strain rates and low confinements. Heating released by the plastic dissipation was highlighted as a potential candidate for hot spot.

In this study, a numerical approach based on a polycrystalline material made of HMX submitted to shear is presented. Due to the confinement during an impact, focus is only put on the heterogeneity arising from anisotropic features and the microstructural characteristics. The behaviour of the binder and the other heterogeneities are set aside. The mechanical dissipation is thus calculated into the volume and the maximum potential temperature is deduced.

## 1. Introduction

In the broad framework of safety studies, the initiation associated with low velocity impact is a recurrent subject among CEA's interests [1-3]. The pyrotechnic reaction relies on a chemical decomposition initiated by the heat flux. Under a low velocity impact, the kinetic energy is scattered through the material. It generates a heterogeneous heating at the microscale on a number of local volumes called "hot spots" where, if a given threshold is reached (critical temperature or energy), the thermal explosion can start. Therefore, predicting initiation requires the investigation of the key mechanisms behind the localization of the kinetic energy. Depending on the material, the localization of the energy is influenced by the micro-structure (particles distribution), the behaviour of the binder and, of course the behaviour of the energetic crystals by themselves. This paper is devoted to this latter topic.

We are working on a pressed energetic material initially made of β-HMX. Its cohesion is improved by a weak fraction of a polymeric binder. Morphologically, it qualifies as a polycristal material with a disperse distribution of the grain sizes. Previous works identified its dissipative deformations mechanisms [4-5]: the intergranular friction, the micro cracking at both inter and trans-granular levels and thus the friction of micro-cracks slips, the viscoelasticity of the binder and the plasticity of the β-HMX crystals. Steven-test experiments made on this explosive composition [3] have shown initiations for projectile velocities in the range of 50 m/s and more. Thus, a confining

pressure of few 100 MPa to 1 GPa is expected. Our assumption is that the confinement inhibits the intergranular sliding by sticking the crystals together. Then, the dissipations due to friction and viscosity of the binder are lowered. It lives us with the crystal plasticity as a dissipative mechanism.

During the impact of a projectile on a target, the kinetic energy first localizes into macroscopic shear bands across the sample, forming macro-cracks. The numerical tools (ABAQUS, Explicit) [6] is used to explore the temperature field generated by the anisotropy of the β-HMX crystals in the vicinity of such cracks. The simulated volume is linked to the investigations of the microstructure on recovered targets showing that the strain laterally spread only few hundred micrometres from the macro-cracks. As a consequence, this work is based on 200 $\mu m^3$ volumes, filled with approximately 68 particles (mean diameter 50µm). Volumes were generated from randomized Voronoi Tessellation. The anisotropy of the stiffness matrix and the slipping systems of the β-HMX are taken from the literature. For each slip system, we use a perfectly plastic criterion and we ignore strain rate dependency [7].

The configuration chosen for the numerical tool is firstly detailed below. Then, material data are listed with the constitutive law implemented in the code. In the third section of this paper, the main results are discussed, the first topic being about the agreement between the mechanical responses of the simulations versus data. Lastly, the discussion is focused on thermal initiation, demonstrating the influence of the plasticity of HMX crystals, when submitted to finite deformation, to the local increase of the temperature.

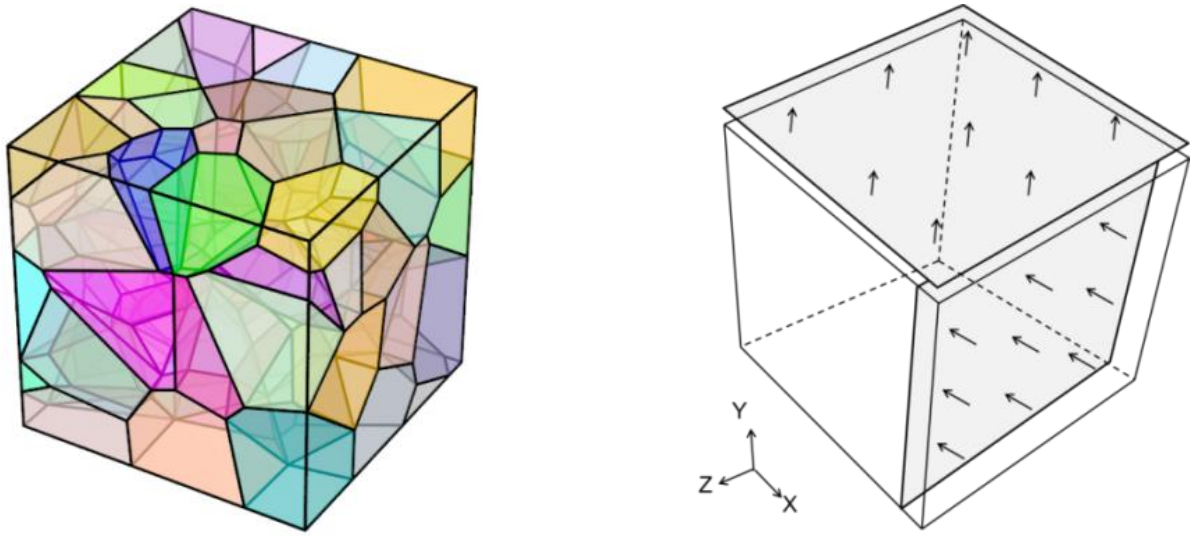


Figure 1 : (Left) One of the Voronoi Tessellation composed of 68 particles. (Right) Constant volume shear loading imposed to the model. The faces left blank are prevented from normal move.

## 2. Calculation procedure

Let us first detail the procedure used to replicate the microstructure of our material. The software NEPER [8] provides randomized Voronoi geometries of 68 particles (Figure 1). Then, GMSH [9] is used to generate a meshed cube of 200 $\mu m^3$ side. OPTIFORM [10] is used to refine and improve the elements with a minimal length of 7 µm. The crystallographic orientation of each particle comes from randomized Euler angles.

The boundary condition reproduces a constant volume shear. On figure 1, the nodes on the white face are prevented from moving out of the plane. A boundary velocity $\dot{a}$ = - 20 m/s is applied on the active face along X. In order to keep a constant volume with a logarithmic deformation, the speed of the active face along Y, denoted $\dot{b}$, is expressed as a function of $\dot{a}$ (eq.**1**).

$$\dot{b} = -\frac{\dot{a}}{a^2} \qquad \textbf{(1)}$$

Finally, the models are sent to ABAQUS (6) which associate the C3D4 formulation to the elements. The constitutive law has been implemented using a VUMAT. The Lagrangian explicit

solver runs for an equivalent time of 4 µs. In the following, a confinement of 800 MPa will be imposed through an increase of the stiffness matrix. As a result, the sound speed in the material is estimated at 2300 m/s, the equilibrium of the forces on opposite faces theoretically being reached after 0.7 µs.

## 3. Material behaviour

### 3.a. Constitutive law of β-HMX crystals

The β-HMX stiffness matrix demonstrates a moderate anisotropy at ambient pressure. Experimental measurements were obtained through Impulsive Stimulated Thermal Scattering [11] and Molecular Dynamic simulations [12] were used to complement and investigate their pressure dependence [13] [14]. A third order polynomial interpolation provides the stiffness coefficient for a confining pressure of 800 MPa (Table **1**).

Table 1 : β-HMX Elastic coefficient at 298 °K and 0 MPa comes from [11]. Data at 800 MPa have been extracted from [13] [15]. The influence of the confinement is highlighted using the Voight-Reuss-Hill equivalent modulus with $\mathbf{K_{VRH}}$ the bulk modulus, $\mathbf{G_{VRH}}$ the shear modulus and $\mathbf{E_{VRH}}$ the Young modulus.

| **Pressure** | $C_{11}$ | $C_{22}$ | $C_{33}$ | $C_{44}$ | $C_{55}$ | $C_{66}$ | $C_{12}$ | $K_{VRH}$ |
|---|---|---|---|---|---|---|---|---|
| 0 MPa | 20.37 | 19.95 | 17.93 | 10.66 | 7.39 | 11.60 | 10.64 | 13.72 |
| 800 MPa | 33.23 | 28.38 | 25.52 | 13.18 | 13.64 | 13.19 | 14.11 | 20.75 |
| **Pressure** | $C_{13}$ | $C_{23}$ | $C_{15}$ | $C_{25}$ | $C_{35}$ | $C_{46}$ | $G_{VRH}$ | $E_{VRH}$ |
| 0 MPa | 9.93 | 13.08 | -1.27 | 5.03 | 1.53 | 5.03 | 6.11 | 15.87 |
| 800 MPa | 16.62 | 20.02 | -2.64 | 6.80 | 1.70 | 6.31 | 8.48 | 22.27 |

HMX crystals accommodate deformation along selected slip systems. The literature yields, for each sliding planes α, a vector $\overrightarrow{m^{\alpha}}$ perpendicular to the plane and expressed in the orthonormal base of the laboratory, and an in-plane vector $\overrightarrow{s^{\alpha}}$. The critical resolved shear stresses (CRSS) are gathered from a Molecular Dynamic simulation [15]. In Table **2**, the systems 3 to 7, and CRSS 1 to 7 were obtained using an optimization algorithm combined with experimental results from gas gunshot on single HMX crystal [15]. The system 1 and 2 were determined by Sheen and Sherwood [16].

Table 2 : The seven slip systems used with CRSS from Barton [15].

| N° | Miller indices $P2_{1/n}$ | Sliding direction $P2_{1/n}$ | Plan $\overrightarrow{m^{\alpha}}$ | | | Direction $\overrightarrow{s^{\alpha}}$ | | | Resolved shear stress[15] GPa |
|---|---|---|---|---|---|---|---|---|---|
| **1** | $(\mathbf{0\,0\,\bar{1}})$ | $\langle\mathbf{1\,0\,0}\rangle$ | **(0,000** | **0,000** | **1,000)** | **<1,000** | **0,000** | **0,000>** | 0,1730 |
| **2** | $(\mathbf{\bar{1}\,0\,\bar{1}})$ | $\langle\mathbf{1\,0\,\bar{1}}\rangle$ | **(0,660** | **0,000** | **-0,751)** | **<0,751** | **0,000** | **0,660>** | 0,0387 |
| 3 | $(\bar{1}\,1\,0)$ | $\langle 0\,0\,1\rangle$ | (0,845 | 0,500 | -0,192) | <0,222 | 0,000 | 0,975> | 0,0722 |
| 4 | $(0\,\bar{1}\,\bar{1})$ | $\langle\bar{1}\,1\,\bar{1}\rangle$ | (0,000 | 0,545 | 0,838) | <0,349 | 0,786 | -0,511> | 0,0959 |
| 5 | $(\bar{1}\,0\,\bar{1})$ | $\langle 0\,\bar{1}\,0\rangle$ | (0,660 | 0,000 | -0,751) | <0,000 | 1,000 | 0,000> | 0,0961 |
| 6 | $(0\,\bar{1}\,\bar{1})$ | $\langle 1\,0\,0\rangle$ | (0,000 | 0,545 | 0,838) | <1,000 | 0,000 | 0,000> | 0,0992 |
| 7 | $(0\,\bar{1}\,0)$ | $\langle 1\,0\,0\rangle$ | (0,000 | 1,000 | 0,000) | <1,000 | 0,000 | 0,000> | 0,1030 |

The constitutive law is based on a hypo-elastic law and an additive decomposition of the total strain rate tensor $\underline{\underline{D}}$:

$$\dot{\underline{\underline{T}}} = \underline{\underline{\underline{\underline{C}}}} : \left(\underline{\underline{D}} - \underline{\underline{D}}^{p}\right) \qquad \textbf{(2)}$$

Where, $\dot{\underline{\underline{T}}}$ denotes the second Polia Kirchhoff stress tensor, $C$ is the stiffness matrix and $\underline{\underline{D}}^{p}$ is the plastic strain rate. The following tensor is used to relate global to in-plane variables:

$$\underline{\underline{m_s^\alpha}} = \frac{1}{2}\left(\overrightarrow{m^\alpha} \otimes \overrightarrow{s^\alpha} + \overrightarrow{s^\alpha} \otimes \overrightarrow{m^\alpha}\right) \quad \textbf{(3)}$$

The latter equation enables determining the resolved shear stress $\tau^\alpha = \underline{\underline{T}} : \underline{\underline{m_s^\alpha}}$ to compute the plastic strain rate based on the plastic slip velocity $\dot{\gamma}^\alpha$ of each plane:

$$\underline{\underline{D^p}} = \sum_\alpha \dot{\gamma}^\alpha sgn(\tau^\alpha) \cdot \underline{\underline{m_s^\alpha}} \quad \textbf{(4)}$$

A quasi-perfect plastic criterion is assumed for each slip system:

$$0 = |\tau^\alpha| - \tau_0^\alpha - \underline{\underline{H}} \cdot \gamma^\alpha \quad \textbf{(5)}$$

Where, $\tau_0^\alpha$ is the CRSS. The tensor *H* incorporates a small uncoupled hardening coefficient (1 MPa) to avoid artificial numerical localizations. Lastly, the elastic response along each slip system must be determined:

$$\Delta\tau^\alpha - \underline{\underline{m_s^\alpha}} : \Delta\underline{\underline{\sigma^p}} + \underline{\underline{m_s^\alpha}} : \sum_\beta \underline{\underline{\underline{\underline{C}}}} : \underline{\underline{m_s^\beta}} \left|\Delta\gamma^\beta\right| sgn\left(\tau_s^\beta\right) = 0 \quad \textbf{(6)}$$

$\Delta\underline{\underline{\sigma^p}}$ being the elastic predictor. For each slip system, this gives us two equations to find the resolved shear stress increment ($\Delta\tau^\alpha$) and shear strain increment $\Delta\gamma^\beta$.

### 3.b. Thermal explosion of HMX-based PBXs

In the context of safety studies, the thermal explosion must be predicted as the first reactive event. Using modified Steven-test targets [3], times to initiation in the order of 10 to few 100 µs were determined on our PBX [17]. Henson *et al.* [18] provided a time/temperature threshold for PBX9501 a HMX-based PBX. Ignition is reached when the temperature increases by 500°K and is maintained during 100 µs. The question is thus the following one: could plasticity generate such an increase of the temperature, neglecting the heat released by the chemical decomposition, during the mechanical loading?

The crystal plasticity provides multiple localized heat sources along few nanometres thick planes spread over seven orientations in the monocrystalline grain. Knowing the diffusivity of the explosive (approximately 0.196x10$^{-6}$ m$^2$/s), a step of temperature suddenly appearing on a null volume propagates through 5.4 µm after 150 µs, a distance well below the minimum finite element size. As a consequence, the thermal conduction is ignored.

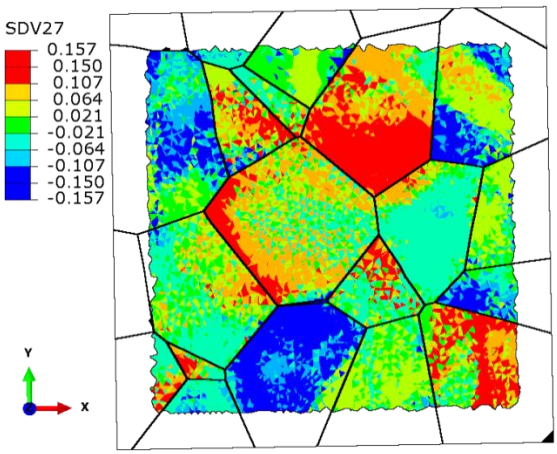


Figure 2: Middle section view of the resolved shear stress for the system 1 in GPa. SDV 27 stands for the plastic deformation of the 1$^{st}$ slipping system. Results plotted on un-deformed mesh.

## 4. Numerical results

This study is based on ten models with elastic and plastic anisotropies ran during 4 µs with a 10 MHz sampling rate, and a model ran during 1 µs with a 100 MHz sampling rate.

Our boundary conditions induce an unwanted additional load which influence can be investigated by removing elements from this area. Removing a 15 µm thick layer yielding a constant temperature on our models, this procedure will be used to extract the temperature and state variables. The Lagrangian solver induces distortion of some elements, the hottest ones being eliminated by the previous procedure.

Deviatoric and volumetric stress and strain are determined on the whole volume. The models show reduced oscillations of the forces between opposite faces of the cubes after 0.58 µs (in accordance with the above theoretical prediction) i.e. a logarithm strain of 0.06.

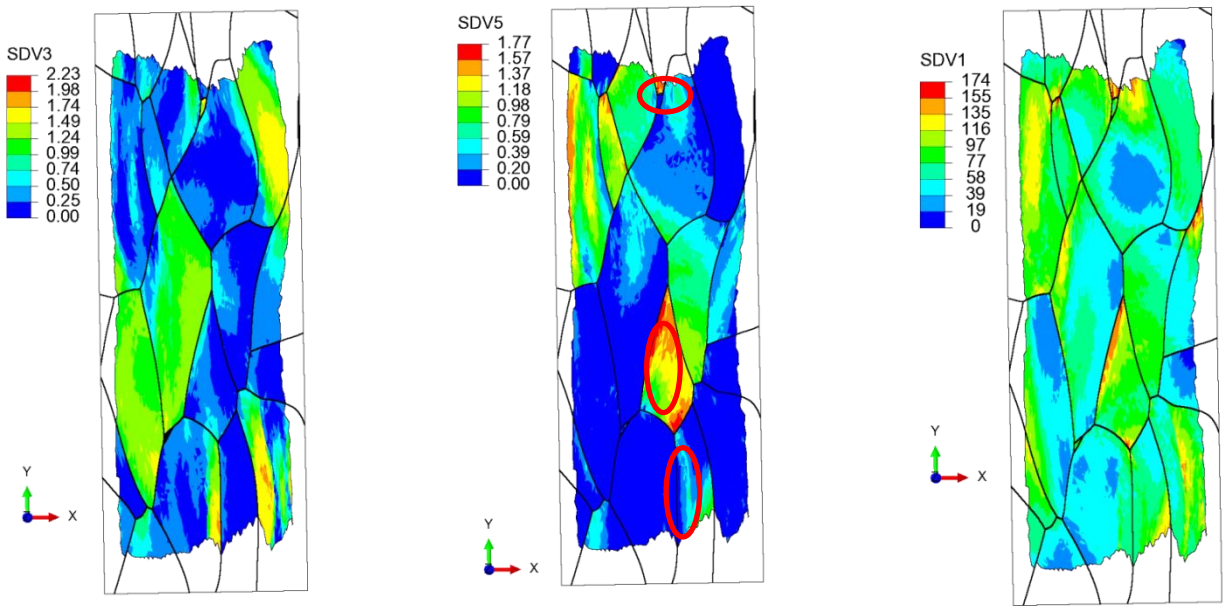


Figure 3: Middle section view of the plastic deformation in system 2 (left), and in system 4 (middle). (right) Map of the temperature increase in °C.

### 4.a. Analysis of a model

A model has been chosen to highlight some local trends of the mechanical and thermal fields. The Figure2 shows the middle section of the model normal to the Z axis. The black lines illustrate the initial grain boundaries when Figure 3 shows their deformation. The Figure2 illustrates the resolved shear stress of the first slipping system with a CRSS of 173 MPa. This is the strongest system and, in this simulation, its yield stress is not reached. However, high elastic stresses are stored, up to 157 MPa (more than the other CRSS). On the opposite, the second slip system, with a CRSS of only 38 MPa, yields the highest plastic strain as shown in Figure 3.

On the figure 3, the contribution of systems two and four to the temperature growth is investigated. Those systems produce the majority of the plastic strain for the polycristal. The location of high plastic strain in system 2 in Figure 3 left (respectively system 4 in Figure 3 middle) rarely correlate (resp. perfectly correlate) with high temperature increase observed in Figure 3 right. Their dissipation depends on the plastic slip and on the CRSS.

In the middle of figure 3, the plastic strain demonstrates a strong heterogeneity maximal near grain boundaries which is also obtained in the middle of figure 3 on the right where the temperature suddenly decreases from 135°C to 39°C across a grain boundary.

The temperature per element collected for each time frame enables determining the maximum, minimum, first decile and quartile and last decile and quartile. On figure 4, the box shows the first and last quartile while the whiskers show the first and last decile. A smooth increase of the median

is observed leading to a “macroscopic” increase of the temperature of approximately 60-70°C. The maximum increase of the temperature is disturbed between 2 and 3 µs, related to a modification of the active slip system due to a reorientation of a grain relative to the load direction. On this same figure, the maximal temperature reaches 250°C with a median and last decile at 65 and 97°C. This illustrates a reduced spread of the temperature with only a few elements able to reach high temperatures. As a consequence, this might lead to localized temperature maximums.

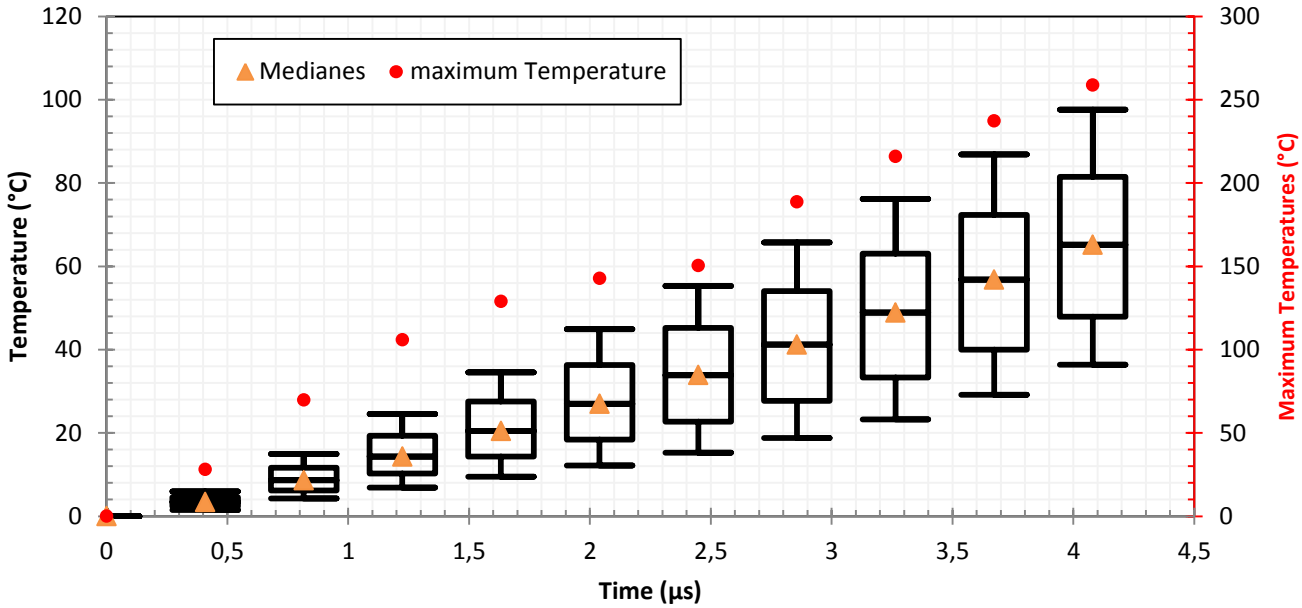


Figure 4: Statistical visualization of the temperature distribution on a model. Orange triangles highlight medians values when the red dots refer to the maximums (right side scale).

### 4.b. Statistical analysis

In this section, the stress-strain response deduced from the simulations is now compared to already existing data. The parameters of the HMX constitutive law have been taken from the literature and no adjustment has been made. The numerical macroscopic deviatoric response is compared to a triaxial experiment made with a confinement of 800 MPa (green curve on Figure 5) [5]. The simulation of a pure anisotropic elasticity (result obtained on a unique model) shows a good agreement with the initial slope of the experiment. It highlights a possible low macroscopic yield stress below 50 MPa which will be investigated in a close future.

The results from the ten simulations are visualized using box and whisker plots. For each simulation, the macroscopic equivalent Von Mises stress is deduced from the normal load at boundaries, yielding ten equivalent stress per time step (strain is deduced from the velocity). A red dot on Figure 5 shows the stress median value and the box highlights the first and third quartiles. The whiskers show the maximum and the minimum stress observed among the ten models. We exclude the first dot due to the equilibrium not being established yet. Compared to experimental results, the median is overestimated by a small margin and the difference in tendencies shows the need for non-negligible hardening coefficient. This observation proves that ten simulations are enough to represent the mean mechanical behaviour of the PBX while the deformation is about 0.15. In a close future, a more statistical study will be made to confirm this conclusion. The equivalent stress asymptote for higher strain will be discussed below.

In this work, we infer a hypothesis on the deformation mechanism mainly based on plasticity rather than damage or internal sliding. The correlation of the numerical stress-strain curve with data enables concluding that for a confinement of 800 MPa and a deformation less than 0.2, the main deformation mechanism is crystal plasticity. The pressure dependence of the CRSS can be neglected up to 800 MPa. The temperature dependence of CRSS already mentioned in [19], [15], [20] will be integrated in a close future.

The experimental equivalent stress still increases when our results show an asymptote. We will add hardening to the plastic deformation of crystals as in [15] [21].

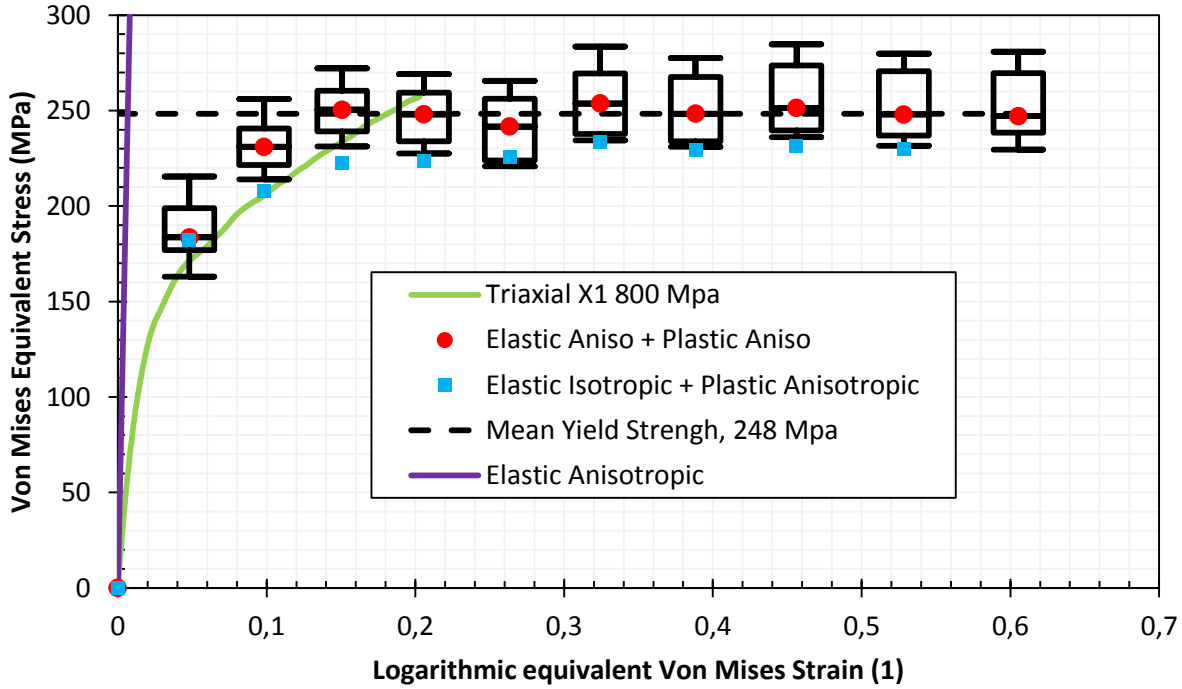


Figure 5: Deviatoric response of the numerical models versus a triaxial data at 800 MPa [5].

Boxes (first and last quartiles) and whiskers (maximum and minimum) are used to illustrate, for the ten models, the distribution of the maximal temperature (Figure 6). Relying on a low number of elements, the maximal temperature increase suffers from a strong variability of ±60°C. Then, during the 4 µs of the simulation (corresponding a strain of 0.6), the maximal temperature reaches 350°C.

Comparing Figure 6 to the same analysis made on the median values enable correlating median and maximal temperatures. An approximately constant ratio of *R*=5.48 is obtained.

A final median temperature increase of 64+/-5°C has been recorded with the ten models when the strain $\Delta\varepsilon_{eq}$ reaches 0.6. Assuming a macroscopic elasto-perfectly plastic and isotropic behaviour as in [3], the global dissipation given by the following relation:

$$\Delta T = \frac{\int_0^{\varepsilon_{eq}^C} \sigma_{eq}^y d\varepsilon_{eq}^{exp} \cdot M_m}{\rho \cdot c_p} + \frac{\sigma_{eq}^y \cdot \left(\varepsilon_{eq}^{max} - \varepsilon_{eq}^C\right) \cdot M_m}{\rho \cdot c_p} - \frac{{\sigma_{eq}^y}^2 \cdot M_m}{2 \cdot P \cdot \rho \cdot c_p} \qquad \textbf{(7)}$$

Yields an increase of 84+/-8°C, close to the previously determined 64+/-5°C, with $\sigma_{eq}^y$=248+/-28 MPa (as shown in Figure 5) and $\rho c_p/\mathrm{Mm}$=1.61x10$^6$ J/m$^3$.K. Due to the absence of equilibrium in the beginning of the numerical model, we integrate over the experimental values up to$\sigma_{eq}^y$ at $\varepsilon_{eq}^C$. Then, the perfectly plastic response is used and the elastically stored energy is removed using the stiffness experimentally measured, P=9815 MPa.

On the temperature difference, we suspect the use of the median instead of a volume weighted mean value. By introducing a correction coefficient $C_{error} = 1.32$ , multiplicative of the numerical temperature, we estimate that a $\varepsilon_{eq}^{500°C} = 0.84$ shear strain is needed to reach the 500°C of the ignition. Reader must remember that a deformation of 0.80 was microscopically observed in samples extracted from unreacted Steven-test target impacted just below the reaction threshold.

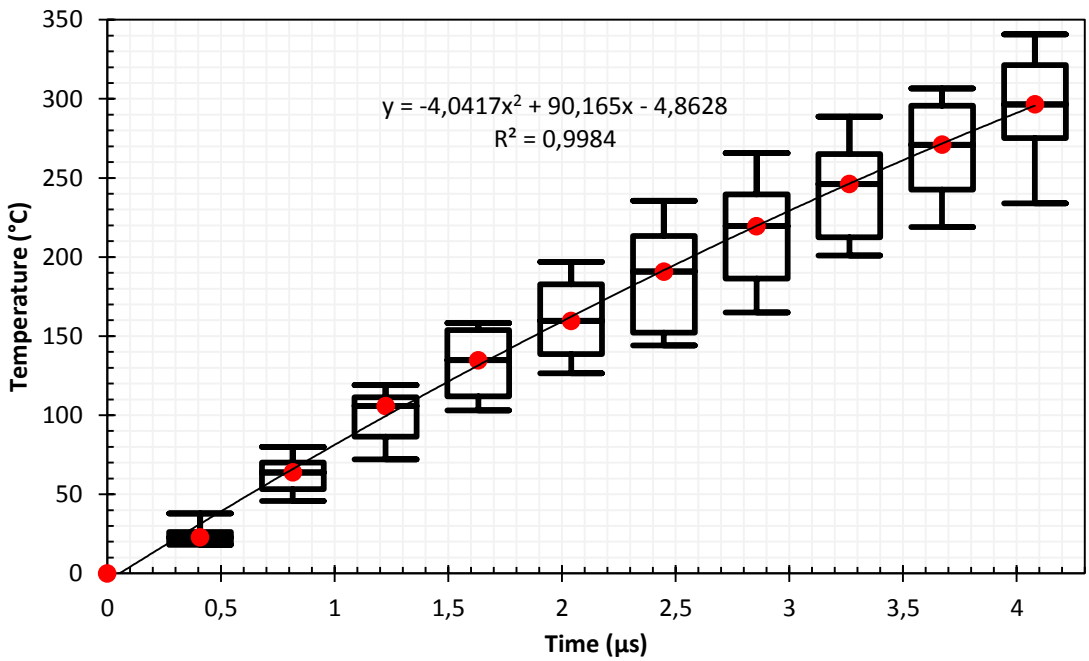

Figure 6: Statistical visualization of the maximal temperature increases over ten models.

## 5. Conclusion

The consequence of low velocity impact on pyrotechnic system is of interest for safety studies. This work addresses an energetic material composed of β-HMX submitted to a dynamic shear loading with the confinement. Attention is focused on the contribution of crystal plasticity dissipation to the initiation of the thermal explosion.

Post mortem examinations showed modifications of the microstructure into shear bands, those thickness approaches few 100 µm, across macro-cracks. A section of those bands has been modelled here. A hypo-elastic perfectly plastic behaviour has been incorporated. The anisotropy of the elastic tensor and those of the plastic slip systems have been used, the parameters being deduced from the literature (no adjustment). Over our numerical results emerges a strong correlation between the median equivalent von Mises stress and data, validating the size of the volume simulated in this paper. It enables identifying the crystal plasticity as the main permanent strain mechanism under confinement (800 MPa) and while the strain is less than 0.4.

Anisotropy of the elastic and plastic behaviours brings a heterogeneous accumulation of plastic strain that leads to strong localized heating. A maximum temperature of 350°C has been obtained for a shear strain of 0.6. An initiation at 500°C requires a plastic shear strain of 0.84 of the same magnitude of the microstructural deformations registered in the bulk of recovered targets submitted to an impact just below the threshold.

Future works will be devoted to (i) numerical improvements, such as adaptive remeshing technics to reduce the interpolation errors, to (ii) the addition of hardening in the plastic behaviour of the slip systems and to (iii) a statistical study, based on many simulations, of the maximum temperature increase.

## Acknowledgements

This study has been carried out within the framework of the Research Laboratory gathering the CEA and the mechanical laboratory Gabriel LaMé.

## References


[1] Vial J., Picart D., Bailly P., Delvare F., Modelling Simul. Mater. Sci. Eng., 21, pp. 16, 2013.
[2] Gruau C., Picart D., Belmas R., Bouton E., Delmaire-Sizes F., Sabatier J., Trumel H., Int. J. of Impact Engineering 36 pp. 537-550.
[3] Picart D., Ermisse J., Biessy M., Bouton E., Trumel H., Int. J. of Energetic Materials and Chemical Propulsion 16 pp. 487-509.
[4] Trumel H., Lambert P., Belmas R., in proc. Int. Detonation Symp. Coeur d'Alene, USA, 2014.
[5] Trumel H., Lambert P., Vivier G., Sadou Y., in *Material under extreme loading. Application to penetration and impact*, eds Wiley & sons, pp. 179-204, 2010.
[6] Software ABAQUS. S.I.: Dassault Systems, 2016.
[7] Biessy M., Picart D., Trumel H., in proc Europyro Tours, France, 2019.
[8] Quey R., *Software Neper: Neper Reference Manual*, 2018.
[9] Geuzaine C., Remacle J.-F., Int. J. for Numerical Methods in Engineering, 79, pp.1309-1331.
[10] Borouchaki H., Grosges T., Barchiesi D., C. R. Mecanique, 338, pp.127-131, 2010.
[11] Sun B., Winey J.M., Gupta Y.M., J. of Applied physics 106, pp. 25-29, 2009.
[12] Sewell T.D., Menikoff R., Bedrov D., *Smith G.,*The Journal Of Chemical Physics, 116, pp.7417-7426, 2003
[13] Mathew N., Sewell T., Propellant, Explosives, Pyrotechnics, 43, pp.223-227, 2018.
[14] Zaug J., Austin R., Armstrong M., Crowhurst J., Goldman N., Ferranti J., Saw C., Swan R., Gross R., Fried L., J. of Applied Physics, 123, 2018.
[15] Barton N., Winter N., Reaugh J., Modelling And Simulation In Materials Sicence And Engineering, 17, pp. 19, 2009.
[16] Sheen D., Sherwood J., Gallagher H., Littlejohn A., Pearson A., Glasgow, University of Strathclyde, 1993.
[17] Picart D., Camus S., in proc Europyro. Tours, France, 2010.
[18] Henson B., Smilowitz L., Asay B., Dickson P., J. Chem. Phys. 117, pp. 3780, 2002
[19] Long Y., Liu Y.G., Nie F.D., Chen J., Philosophical Magazine92:8, pp.1023-1045, 2012.
[20] Khan M., Pal A., Picu C., Modelling Simul. Mater. Sci. Eng., 26, pp.15, 2018.
[21] Austin R., Barton N., Reaugh J., Fried L., J. of App. Phys. 117, 2015.